Atmospheric Environment 142 (2016) 420–429

Contents lists available at ScienceDirect

Atmospheric Environment

journal homepage: www.elsevier.com/locate/atmosenv

Vertical mass impact and features of Saharan dust intrusions derived from ground-based remote sensing in synergy with airborne in-situ measurements

Carmen Córdoba-Jabonero [a, *], Javier Andrey-Andrés [a, 1], Laura Gómez [a, 2], José Antonio Adame [a], Mar Sorribas [a], Mónica Navarro-Comas [a], Olga Puentedura [a], Emilio Cuevas [b], Manuel Gil-Ojeda [a]

[a] Instituto Nacional de Técnica Aeroespacial (INTA), Atmospheric Research and Instrumentation Branch, Ctra. Ajalvir km. 4, Torrejón de Ardoz, 28850, Madrid, Spain

[b] Agencia Estatal de Meteorología (AEMET), Atmospheric Research Centre of Izaña, Sta. Cruz de Tenerife, Spain

HIGHLIGHTS

- Synergy between airborne and Lidar observations for Saharan dust vertical mass impact.
- Optical and microphysical properties reported for Saharan Air Layer characterization.
- Higher dust incidence in FT w.r.t. BL regarding particle fine and coarse size modes.
- Assuming averaged MEE is critical in mass concentration estimation of single layers.
- Good agreement in vertical extinction retrieval between MAXDOAS and LIDAR profiling.

GRAPHICAL ABSTRACT

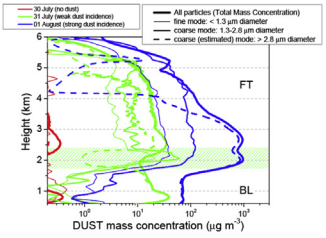

ARTICLE INFO

Article history:
Received 9 December 2015
Received in revised form
25 June 2016
Accepted 1 August 2016
Available online 4 August 2016

Keywords:
Airborne measurements
Air quality impact
Dust
LIDAR

ABSTRACT

A study of the vertical mass impact of Saharan dust intrusions is presented in this work. Simultaneous ground-based remote-sensing and airborne in-situ measurements performed during the AMISOC-TNF campaign over the Tenerife area (Canary Islands) in summertime from 01 July to 11 August 2013 were used for that purpose. A particular dusty (DD) case, associated to a progressively arriving dust intrusion lasting for two days on 31 July (weak incidence) and 01 August (strong incidence), is especially investigated. AERONET AOD and AEx values were ranging, respectively, from 0.2 to 1.4 and 0.35 to 0.05 along these two days. Vertical particle size distributions within fine and coarse modes (0.16–2.8 μm range) were obtained from aircraft aerosol spectrometer measurements. Extinction profiles and Lidar Ratio (LR) values were derived from MPLNET/Micro Pulse Lidar observations. MAXDOAS measurements were also used to retrieve the height-resolved aerosol extinction for evaluation purposes in comparison to Lidar-derived profiles. The synergy between Lidar observations and airborne measurements is established in

* Corresponding author.
E-mail address: cordobajc@inta.es (C. Córdoba-Jabonero).
URL: http://www.inta.es/atmosfera
[1] Now at: CNRM-GAME, Météo-France and CNRS, Toulouse, France.
[2] Also at: Groupe de Spectrométrie Moléculaire et Atmosphérique, URM CNRS 7331, UFR Sciences Exactes et Naturelles, Reims, France.

http://dx.doi.org/10.1016/j.atmosenv.2016.08.003

Mass efficiency
MAXDOAS

terms of the Mass Extinction Efficiency (MEE) to calculate the vertical mass concentration of Saharan dust particles. Both the optical and microphysical profilings show dust particles mostly confined in a layer of 4.3 km thickness from 1.7 to 6 km height. LR ranged between 50 and 55 sr, typical values for Saharan dust particles. In addition, this 2-day dust event mostly affected the Free Troposphere (FT), being less intense in the Boundary Layer (BL). In particular, rather high Total Mass Concentrations (TMC) were found on the stronger DD day (01 August 2013): 124, 70 and 21 μg m^{-3} were estimated, respectively, at FT and BL altitudes and on the near-surface level. This dust impact was enhanced due to the increase of large particles affecting the FT, but also the BL, likely due to their gravitational settling. However, the use of an assumed averaged MEE value can be especially critical for estimating the mass concentration of particular layers. Moreover, the potential of MAXDOAS retrieval for aerosol extinction profiling is also evidenced by showing a relatively good agreement with the Lidar-derived extinction profiles, once a particular smoothing procedure is applied to Lidar measurements.

1. Introduction

The vertical distribution of dust plays a significant role in climate-related issues, in particular those associated to its atmospheric radiative forcing (Boucher et al., 2013; Myhre et al., 2013). In addition, height-resolved information of the dust properties is required for both aerosol transport modelling (i.e., de la Paz et al., 2013; Zhang et al., 2013), particularly relevant for particle deposition estimation (Schepanski et al., 2009), and satellite data validation (i.e., Campbell, et al., 2012; Amiridis et al., 2013). In order to obtain this information, a general effort is being made by the ESA (European Space Agency) Earth Observation programs related to the next future Copernicus/Sentinel and EarthCARE (Earth Cloud-Aerosol-Radiation Explorer) missions focused on the vertical monitoring of aerosols and clouds and the retrieval of their macro/microphysical and optical properties for assessment of both the air quality impact and radiative forcing concerns.

Canary Islands offer a suitable region for Saharan dust monitoring, as located downwind of the Sahara desert. The arrival of dust plumes are frequent in this area, mainly in summertime and extended up to high altitudes (Córdoba-Jabonero et al., 2014, 2016). The vertical characterization of individual dust events is relevant for the determination of the so-called Saharan Air Layer (SAL), defined as a mass of warm and dusty air, in order to evaluate the climate impact of such phenomena, even at local scales (Carlson and Prospero, 1972). Indeed, extended campaigns have been carried out over this region and surroundings specially focused on dust research; in particular, both AMMA 2006 (African Monsoon Multidisciplinary Analysis, Formenti et al., 2011) and SAMUM 2006 and 2008 (Saharan Mineral Dust Experiment, Ansmann et al., 2011 and reference therein) must be mentioned for their relevance in desert dust characterization using both ground-based and airborne observations.

In this sense, the AMISOC (Atmospheric Minor Species relevant to the Ozone Chemistry) project was planned as a multi-instrumented campaign (AMISOC-TNF) carried out, particularly, over Tenerife area (Canary Islands, Spain) in summertime. The main goal was the study of the behaviour of minor traces gases under clean skies and heavy aerosol loading as well as the dust impact in air quality and climate-related issues. Among all AMISOC activities, a particular emphasis was put on dust profiling. Indeed, this study reflects the synergy of airborne in-situ instrumentation (Optical Particle Counters, OPC) and ground-based active (LIDAR) techniques to derive, respectively, the height-resolved microphysical and optical properties of particles in the SAL. In addition, the available MAXDOAS (Multi-AXis Differential Optical Absorption Spectrometry) measurements during AMISOC-TNF were also used to retrieve the height-resolved aerosol extinction.

The Total Mass Concentration (TMC) of dust particles, regarding their radiative impact factor, can be also estimated in terms of the Mass Extinction Efficiency (MEE). MEE is a measure of the aerosol effectiveness on solar radiation, relating both optical and microphysical properties. In general, MEE values as reported in the Optical Properties of Aerosols and Clouds (OPAC) database (d'Almeida et al., 1991; Tegen and Lacis, 1996; Hess et al., 1998; www.pole-ether.fr) are higher for smaller particles. Indeed, MEE for dust decreases as effective particle radius increases. Values of 3.1–2.3 m^2 g^{-1} and 0.97–0.16 m^2 g^{-1} are obtained for dust particle size distributions with effective radius within the fine and coarse modes, respectively (see OPAC database, www.pole-ether.fr). In particular, MEE values of 0.5, around 1.0 and 1.09 m^2 g^{-1} were obtained from in-situ measurements performed in close regions to Saharan dust sources as Izaña/Tenerife site (Maring et al., 2000), Morocco (SAMUM, 2006; Kandler et al., 2009) and Cape Verde (AMMA campaign, Chen et al., 2011), respectively, likely in average depending on the different contribution of fine (higher MEE) and coarse (lower MEE) particles. In addition, MEE values of 0.75 and 0.80 m^2 g^{-1} were assumed for campaigns carried out in more distant areas as Puerto Rico (during the Puerto Rico Dust Experiment-PRIDE campaign, Reid et al., 2003) and Barbados (Li et al., 1996), respectively. That previous work reported in Reid et al. (2003) shows the dust vertical profiling during the PRIDE airborne campaign, devoted to the transcontinental transport of Saharan dust particles. An emphasis is put on the vertical distribution, using similar airborne instrumentation as that used in AMISOC-TNF. Whereas Reid et al. (2003) mostly focused on dust particles present over the Caribbean region after their long-range transport from the African continent, our study is mainly motivated on the detection of Saharan dust after short-range transport of dust particles from their African source regions.

Therefore, the aim of this work is twofold: (1) to examine the vertical features of both the dust Lidar-derived optical properties (e.g., extinction coefficients and LR) and the microphysical properties (e.g., particle size distributions and fine/coarse mode (fm/cm) predominance) obtained from airborne in-situ measurements; and (2) to study the potential of combined Lidar and airborne observations in estimating the mass concentration of Saharan dust particles and their vertical incidence with implications in the air quality and health. In addition, the also available passive MAXDOAS-derived extinction profiles are also evaluated in comparison with those retrieved from active Lidar measurements in order to show the potential of this technique lately also used to derive the aerosol extinction profiling. In general, single/multi-layered dust structure, SAL top height, dust incidence in both Free Troposphere (FT) and Boundary layer (BL), Lidar Ratio (LR) estimation, and particle fm/cm predominance are the main aspects

examined.

All the methodology used in this work is described in Section 2. Section 3 presents the results obtained and their discussion in relation with: 1) the description of the dusty conditions occurred along the overall AMISOC-TNF campaign; 2) the vertical features of a progressively arriving Saharan dust intrusion lasting two days regarding its weak and strong BL/FT incidence; 3) the mass concentrations of dust particles found during that 2-day dust intrusion; and 4) the evaluation of the MAXDOAS extinction profiles. Main conclusions are introduced in Section 4.

2. Methodology

2.1. AMISOC-TNF sampling area

Simultaneous aerosol vertical observations were carried out over the Canary Islands region by using both airborne in-situ and ground-based (GB) active and passive remote sensing measurements.

GB instrumentation was deployed at Tenerife Island (one of the Canary Islands, Spain) in two stations: the Sta. Cruz de Tenerife observatory (SCO, 28.5°N 16.3°W, 52 m a.s.l.) and the Izaña observatory (IZO, 28.3°N 16.5°W, 2373 m a.s.l.), both managed by the Spanish Meteorological Agency (Agencia Estatal de Meteorología, AEMET). They are located at about 40 km distance each other, and around 1000 km far from Saharan dust sources (Córdoba-Jabonero et al., 2011; see Fig. 1). Both stations are AERONET (AErosol RObotic NETwork, aeronet.gsfc.nasa.gov) sites, and in particular SCO is also a MPLNET (MicroPulse Lidar NETwork, mplnet.gsfc.nasa.gov) site.

Airborne measurements were carried out aboard the INTA/C212 aircraft (INTA, Instituto Nacional de Técnica Aeroespacial/Spanish Institute for Aerospace Technology). This aerial platform performed six flights during AMISOC-TNF campaign under both non-dusty (ND) (4 flights) and dusty (DD) (2 flights) conditions. In particular, the selected dust intrusion event examined in this work corresponded to the aircraft flights performed on 31 July and 01 August 2013 (see Section 3.1). The flight carried out on 30 July 2013 (clean day) was used as a reference under ND conditions. On these days, the flight trajectory followed by the aircraft consisted on ascent and descent vertical spirals between the islands of Tenerife and Las Palmas de Gran Canaria. 11 straight level runs (SLR) at constant height were inserted into the descent spiral at different heights. The vertical speed was fixed to 3 m/s to maximize the number of measurements. The altitude range was from 100 m to around 6500 m a.g.l., and the time window was between 09:30 and 12:30 UTC lasting 2 h, approximately.

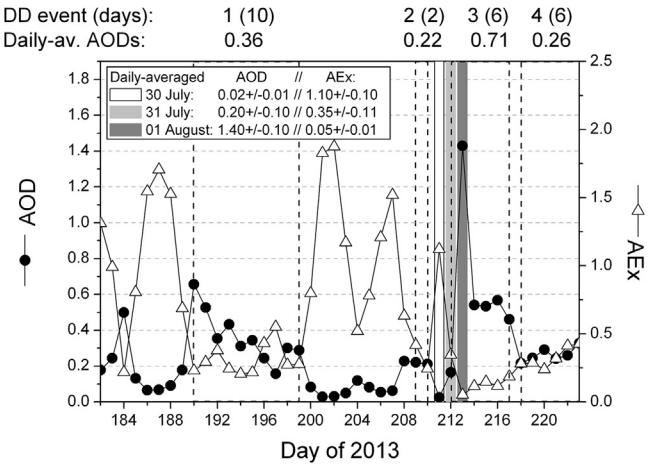

Fig. 1. Temporal evolution of AERONET daily-averaged AOD (full circles) and AEx (open triangles) values during AMISOC-TNF campaign. The four observed DD periods are highlighted (detached by dashed lines), indicating also their mean AOD and day-length (in brackets). Aircraft flights are also shown by white/grey bands.

2.2. Airborne in-situ instrumentation

Aerosol size distributions (SD) at several size ranges were obtained by using an optical particle counter (OPC), the Passive Cavity Aerosol Spectrometer Probe (PCASP-100X), manufactured by Droplet Measurements Systems (DMS, see more details in Baumgardner et al., 2001). The PCASP spectrometer was mounted in a pod under the wing of the INTA/C212 aircraft during AMISOC-TNF; PCASP is similar to that also used in other airborne campaigns: AMMA (Formenti et al., 2011), SAMUM (Weinzierl et al., 2009) and PRIDE (Reid et al., 2003).

In general, PCASP instrument classifies the aerosol particles into several size channels, being the nominal size range between 0.1 and 3.0 μm diameter. Regarding the refractive index of the dust particles, the size range of each channel is adjusted respect to that value used in calibrations. A representative refractive index for Saharan dust of 1.49 (Schuster et al., 2012), neglecting the absorption, is assumed. Hence, PCASP SDs were detached in 13 channels with an overall particle size range of 0.1–3.3 μm diameter. However, as usually for OPCs, the first and last PCASP channels are excluded from our analysis (as exposed in Reid et al., 2003), leaving an operational size range between 0.16 and 2.8 μm particle diameter. Single size channels of this interval were selected and assembled into three 'wider' size ranges in order to examine particles within both fine and coarse modes. Accounting for the AERONET cut-off size between these two particle modes (0.6 μm radius), PCASP channels 3–6, 7–10 and 11–12 were grouped, corresponding, respectively, to the fine 0.16–0.34 μm (D1) and 0.34–1.34 μm (D2) diameter-size ranges and the 1.34–2.83 μm (D3) size range for particles within the coarse mode. Despite coarse particles larger than those measured by PCASP are also present under Saharan dust intrusion occurrence (i.e., Weinzierl et al., 2009), the analysis of particles within these three D1-D3 size fractions is especially relevant for studies on aerosol radiative effect. Indeed, MEE values for dust (see OPAC database, d'Almeida et al., 1991; Tegen and Lacis, 1996; Hess et al., 1998) are higher for smaller particles.

SD calculations were performed by applying those algorithms used in Molero et al. (2014) to PCASP measurements, reporting accuracies in size estimation and aerosol concentration of 16% and 20%, respectively (Baumgardner et al., 2005). The PCASP measuring principle and uncertainties are described in detail in Rosenberg et al. (2012) and Cai et al. (2013) (and references therein). Number SDs (NSD, cm^{-3}) and volume SDs (VSD, $\mu m^3\ cm^{-3}$) profiles for particles within those D1, D2 and D3 size ranges were obtained.

2.3. Ground-based remote sensing instrumentation

Aerosol GB measurements were performed by using both active and passive remote sensing (RS) instrumentation.

2.3.1. Active RS: MPLNET Micropulse Lidar

The Micro Pulse Lidar v. 3 (MPL-3) is a standard system of those that are running within the NASA/MPLNET, and routinely operated at SCO site since 2005. The MPL-3 system is managed by the INTA/Atmospheric Research and Instrumentation Branch (INTA/AIIA, www.inta.es/atmosfera) in collaboration with AEMET. The MPL-3 features can be summarized as follows (see Campbell et al., 2002; Córdoba-Jabonero et al., 2011; for more details): eye-safe laser beam at 523 nm, energy pulse of 7–8 μJ, pulse repetition frequency of 2500 Hz, and 20-cm diameter of telescope-receiver system. Lidar

measurements were registered with a 15-m vertical resolution and 1-min integrating time, and the range-corrected signal (RCS) profiles were hourly-averaged.

Optical properties of the Saharan dust particles are derived from Lidar measurements by using the inversion procedure described in Córdoba-Jabonero et al. (2014). In short, both vertically-resolved extinction coefficients and the Lidar Ratio (LR, extinction-to-backscatter ratio) are retrieved by using a modified version of the Klett-Fernald elastic Lidar inversion algorithm (Fernald, 1984; Klett, 1985) by constraining the height-integrated extinction with AERONET sun-photometer AOD data obtained at both SCO and IZO stations.

2.3.2. Passive RS: AERONET sun-photometry

NASA/AERONET sun-photometers are located at both SCO and IZO sites. Columnar-integrated AOD at 500 nm and Angstrom Exponent (AEx) at the 440/675 nm wavelength pair are used for two proposes: (1) AOD constrain is required in the elastic lidar retrieval algorithm to obtain the extinction profiles and LR values (Córdoba-Jabonero et al., 2014), as exposed before; and (2) selection of the DD cases observed during AMISOC-TNF campaign. These two parameters are usually used for dust identification (Holben et al., 2001; Toledano et al., 2007a,b) within a particular interval of AOD and AEx values. Dust intrusions are usually detected by observing AOD increases simultaneously with AEx decreases down to near-zero values.

In particular, DD conditions during the AMISOC-TNF campaign were identified by using our experience about AOD data at the sampling site with the criterion for dust particles adopted in Córdoba-Jabonero et al. (2011), where a Saharan dust intrusion transported over the same study zone of this work was monitored and analyzed. This criterion is based on AERONET AOD and AEx data at SCO site for evidence of the predominance of coarse particles (dust intrusion conditions): high-moderate AOD (>0.2) and low AEx (<0.5) were defined as threshold DD values that represent dusty conditions in the Tenerife area. AERONET data at the AEMET/IZO station, representative for background FT sites (as located at 2367 m a.s.l.), were also used for identifying differences in vertical dust loading, in particular, between the BL and FT.

2.3.3. Passive RS: MAXDOAS spectroscopy

Multi-Axis Differential Optical Absorption Spectroscopy (MAXDOAS) observations were also performed over IZO site during AMISOC-TNF campaign using the MAXDOAS spectrometer settled in the framework of NDACC (Network for the Detection of Atmospheric Composition Change) at IZO in 2010. Detailed description of the instrument can be found in Gil et al. (2008) and Puentedura et al. (2012). MAXDOAS is a passive RS technique for the measurement of atmospheric gases mixing ratios, based on the spectrum of diffuse solar radiation recorded by a DOAS spectrometer pointing at several observational angles (multi-axis observations) (Platt and Stutz, 2008). The MAXDOAS spectrometer used in this work recorded the sky spectrum in the visible range with a spectral resolution of 0.55 nm at 10 elevation angles from −1° to 90° respect to the horizon, and was fixed pointing to North (0° azimuth); the field of view was 1°, and a full cycle was covered in 20 min. The analysis of these measurements provides the slant column density (SCD) for a given gas, defined as the density of the gas integrated along the optical path. The retrieval procedure for the SCD calculation from MAXDOAS measurements is the same as shown in Gil et al. (2008) for DOAS observations. In particular, the aerosol profiles are retrieved from the O_4 SCD measured at different elevation angles. Hence, O_4 SCDs are routinely evaluated in the standard spectral 425–520 nm range defined by NDACC for NO_2, since O_4 presents a strong absorption band at 477 nm.

O_4-based MAXDOAS measurements are used in combination with a radiative transfer model inversion algorithm to retrieve the aerosol vertical profiles (Wagner et al., 2004; Friess et al., 2006) by using the Optimal Estimation Method (OEM) (Rodgers, 1990). In the linear case (retrieval of trace gas profiles) (e.g., Clémer et al., 2010; Hendrick et al., 2014), given a set of measurements $\boldsymbol{y}$ with the error covariance $\mathbf{S}_\epsilon$, the OEM provides the state vector $\boldsymbol{x}$ that maximizes the probability that $\boldsymbol{x}$, containing the trace gas vertical distribution, belongs to the interval $[\boldsymbol{x}, \boldsymbol{x} + \boldsymbol{dx}]$. Applying OEM approach, the maximum a posteriori solution $\hat{x}$ is calculated by the following expression:

$$\hat{x} = x_a + S_a K^T \left(K\, S_a K^T + S_\in\right)^{-1} (y - K x_a) = x_a + G_y (y - K\, x_a) \tag{1}$$

where the weighting function matrix $\mathbf{K}$ refers to the sensitivity of the measurements to variations in the trace gas profile. The $\boldsymbol{x_a}$ vector and $\mathbf{S_a}$ matrix correspond to an a priori gas profile and its corresponding error covariance matrix, respectively.

A similar procedure can be applied to obtain the vertical aerosol extinction profile. This procedure (e.g., Wagner et al., 2004; Friess et al., 2006; Clémer et al., 2010) is based on the fact that the concentration of the oxygen dimmer (O_4) is known and stable in the atmosphere. Hence, a variation in their DSCDs is commonly related to a change of the optical path, usually associated to the presence of aerosols. In this case, the problem is non-linear ($\mathbf{K}$ is independent on $\boldsymbol{x}$), and then the aerosol extinction profile is obtained by using an iterative process.

2.4. HYSPLIT backtrajectory analysis

Three-dimensional kinematic backtrajectories were calculated using HYSPLIT (Hybrid Single Particle Lagrangian Integrated Trajectory) model (Draxler et al., 2009) to identify the Saharan origin of the air masses. The ECMWF (European Centre for Medium Range Weather Forecasts) meteorological fields with a spatial resolution of 0.25° × 0.25° were used, with 22 vertical levels from the surface to 250 mb and a time resolution of 6 h. Hourly backtrajectories with a five-day (120 h) pathway were computed. In order to investigate the lower and middle troposphere, five altitudes were selected: 500 m (close to the surface), 1000 m (representative of the BL top), 2000 and 3000 m (at FT altitudes) and 5000 m (above IZO station).

2.5. Calculation of the total mass concentration for Saharan dust particles

NSDs and VSDs were obtained from PCASP measurements (see Section 2.2) carried out by the aircraft flights performed during AMISOC-TNF.

The Mass Concentration (MC) was calculated for particles within each selected size range (D_i, i = 1, 2, 3) by using the expression:

$$MC(D_i) = d_p \times VSD(D_i) \tag{2}$$

where d_p is the particle density (a value of 2.0 g cm^{-3} is assumed, Reid et al., 2003; Córdoba-Jabonero et al., 2011), and VSD(D_i) are the integrated VSD of all particles within each 'wide' D1, D2 and D3 channels registered by PCASP (see Section 2.2). Hence, height-resolved variations of the mass concentration of dust particles can be obtained for both particle fine (D1 + D2) and partial coarse (D3) modes. In addition, once the MC is calculated for the overall D1 + D2 + D3 size range (particles with sizes smaller than 2.8 μm diameter), the MC for larger particles with diameter greater than 2.8 μm (i.e., particles within the labelled D4 size range hereafter)

can be also estimated by subtracting the MC (D1 + D2 + D3) from the Total Mass Concentration (TMC) for all the particles.

The Total Mass Concentration for all the particles (TMC, g m^{-3}) can be obtained by using its intrinsic relation with the optical extinction in terms of the Mass Extinction Efficiency (MEE, m^2 g^{-1}), i.e., following the expression:

$$\sigma^{ext} = MEE \times TMC \quad (3)$$

where σ^{ext} (m^{-1}) is the extinction coefficient. Hence, a vertical estimate of the TMC can be calculated from Lidar-derived σ^{ext} profiles in combination with an averaged value assumed for MEE. Several MEE values are reported for dust in the literature, either obtained from in-situ measurements or assumed, as mentioned in the Introduction. Table 1 shows a brief overview of those reported MEE values for dust together with related information.

In particular, among those values, a MEE of 1.0 m^2 g^{-1} is assumed for TMC calculations in this work, as that reported during SAMUM campaign performed over the nearest region to our sampling area (see Table 1). The vertical estimate of mass concentrations for Saharan dust particles in both fine and coarse modes is also analyzed.

3. Results and discussion

3.1. Saharan dust occurrence during AMISOC-TNF campaign

AMISOC-TNF campaign was carried out from 01 July to 11 August 2013 (42 days in summertime). 24 days (57.1% of total) were identified as dusty (DD) cases (see Section 2.3). Regarding IZO dusty features for the overall period, the mean percentage of AOD over IZO (AOD^{IZO}) respect to the total AOD (referred to the AOD over SCO, AOD^{SCO}) was 49 ± 19%, besides the AEx values over IZO were lower than 0.5 (coarse particles predominance) for all those 24 DD days. This result indicates the arrival of dust intrusions at high altitudes, as expected in summertime over this region.

Fig. 1 shows the temporal evolution of the daily-averaged AOD and AEx values over SCO site during AMISOC-TNF campaign, observing four DD periods with a mean AOD higher than 0.2 and lasting between 2 and 10 days. In addition, aircraft flights were performed under clean ND conditions on 30 July 2013, and DD loading on 31 July and 01 August 2013 (shown by white/grey bands in Fig. 1). Hence, regarding simultaneous GB remote sensing and airborne measurements, that particular 2-day DD event occurred on 31 July and 01 August 2013 was selected to be examined in more detail in this work.

This 2-day DD event corresponded to a progressively arriving Saharan dust intrusion over Tenerife area on 31 July with weak incidence, lasting on 01 August with a much stronger impact. AERONET AOD and AEx values ranged, respectively, from 0.2 to 1.4 and 0.35 to 0.05 for these two days. ND loading conditions present during the previous day on 30 July 2013 with mean AOD/AEx values of 0.02/1.1 were also considered as a reference.

Both ND and DD conditions were also confirmed by backtrajectory analysis. Fig. 2 shows HYSPLIT 5-day backtrajectories of the air masses ending at 11:00 UTC (closest time to the aircraft flights) over SCO site on 30 July, 31 July and 01 August 2013. Their arrivals are shown at five altitudes (m a.g.l.): 500, 1000, 2000, 3000 and 5000 (see Section 2.4 for details).

ND conditions observed on 30 July 2013 are reflected by the HYSPLIT backtrajectories, showing clean air masses mostly coming from the Atlantic Ocean region at all those altitudes (see Fig. 2, left). On 31 July 2013 from 00:00 UTC on (data not shown), a weak dust intrusion is progressively coming, mainly observed at high levels (around 5000 m a.g.l.), with a relatively low mean AOD of 0.17 but also a low AEx value of 0.35 (coarse particles signature). Backtrajectories at the closest time of the aircraft measurements indicate air masses mostly arriving from Atlantic Ocean at atmospheric levels lower than 5000 m a.g.l. (see Fig. 2, centre). The arrival of dust particles is observed on 31 July from 12:00 UTC on over 3000 m a.g.l. This situation continues on 01 August 2013, with increasing dust loading; hence, a strong dust intrusion is occurring along this day (see Fig. 2, right). Indeed, results obtained by backtrajectory analysis indicate Saharan air masses coming in a layer confined mostly between 2000 and 5000 m a.g.l., while no dust incidence is observed at lower BL layers with cleaner Atlantic Ocean air masses arrivals.

3.2. Vertical profiling features and dust incidence

Simultaneous Lidar-derived extinction profiles together to airborne vertical SDs are analyzed during the 31 July-01 August period, corresponding to weak and strong DD conditions, respectively (30 July case is also examined as a background ND reference). Fig. 3 shows the vertical profiling of the MPL-3 extinction coefficients and the PCASP integrated NSD for particles registered within D1, D2 and D3 size ranges on 30 July, 31 July and 01 August 2013. Since aircraft measurements were carried out for 1–2 h between 10:00 and 12:00 UTC, hourly-averaged extinction profiles are shown at 10:00–11:00 UTC and 11:00–12:00 UTC (see Fig. 3, solid and dashed lines, respectively).

In general, a wide dust layer is observed between 1.7 and 6 km height with respect to previous ND conditions (30 July), being much stronger on 01 August (see Section 3.1). Indeed, dust incidence mostly affected FT altitudes with almost no incidence in the BL (BL top height is reached at around 1200 m a.s.l.), as reflected by both lidar and airborne measurements (see Fig. 3). In particular, dust extinction in the FT increases 7 and 140 times in average on 31 July and 01 August, respectively, with respect to values for ND case; however, the BL extinction increase is only 1.4 and 3.7 times higher. Similar results are obtained for NSD data. Table 2 shows the extinction and NSD increases at both FT and BL layers obtained on 31 July and 01 August with respect to those values registered on 30 July (dust particles are detached in the fine D1 and D2 and partial coarse D3 PCASP channels). Indeed, the amount of dust D3 particles is enhanced mostly at FT heights, while the enhancement of fine D1

Table 1
Averaged MEE values reported for Saharan dust particles (sampling sites and references are also included).

MEE (m^2 g^{-1})	Site (region)	Reference
0.50[a]	Tenerife (Canary Islands, IZO site, 2400 m a.s.l.)	Maring et al. (2000)
0.75	Puerto Rico (Caribbean region, PRIDE campaign)	Reid et al. (2003)
0.80	Barbados (Caribbean region)	Li et al. (1996)
0.88	SW Iberian Peninsula (INTA/El Arenosillo atmospheric observatory, ARN)	Córdoba-Jabonero et al. (2011)
1.00	Morocco (North Africa, SAMUM, 2006 campaign)	Kandler et al. (2009), Weinzierl et al. (2009)
1.09	Cape Verde (Africa, AMMA campaign)	Chen et al. (2011)

[a] Mass Scattering Efficiency (MSE).

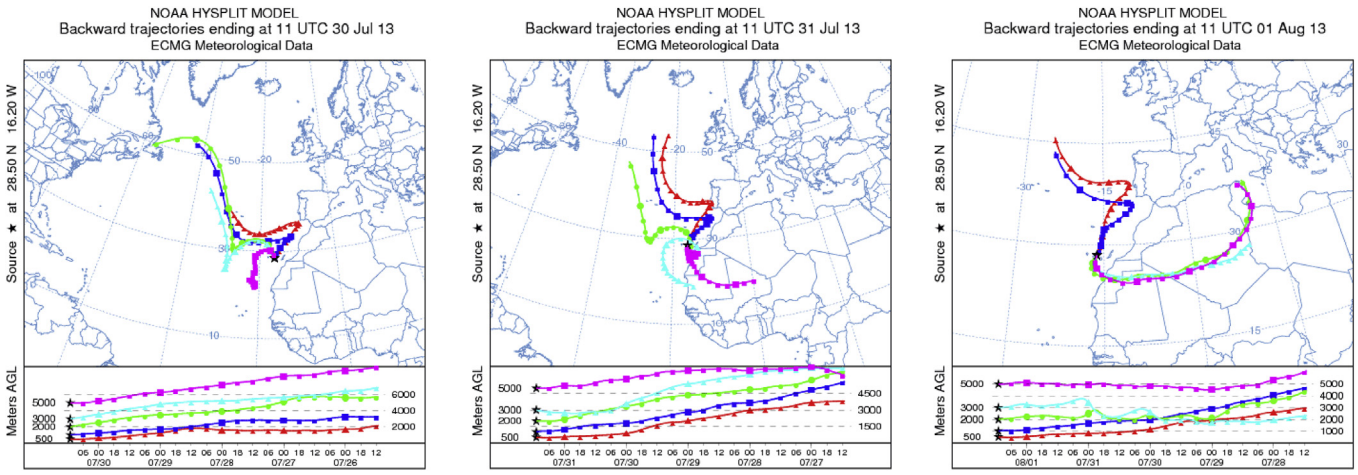

Fig. 2. HYSPLIT 5-day backtrajectories ending at 11:00 UTC (closest time to aircraft flights) over SCO site on 30 July (left), 31 July (centre) and 01 August (right). Five altitudes (m a.g.l.) of the arrival of the air masses are shown: 500 (red), 1000 (blue), 2000 (green), 3000 (light blue) and 5000 (pink). (For interpretation of the references to colour in this figure legend, the reader is referred to the web version of this article.)

and D2 particles remains at similar values for the two DD days (see Fig. 3 and Table 2). Note the increase of larger (D3) particles in the BL from 31 July to 01 August, likely due to gravitational processes from higher altitudes. The observed enhancement of Saharan dust particles mainly in the FT, as also shown by backtrajectory analysis (see Section 3.1), reveals the large extinction observed also at those altitudes. In particular, this is especially marked on 01 August (strong dust intrusion case), since the scattering is an extensive aerosol property depending directly on the particle number.

Regarding the LR for this 3-day period (see Table 2), the ND case with air masses coming from the Atlantic Ocean (as indicated by HYSPLIT backtrajectory analysis, see Section 3.1), reported a daily-averaged LR value of 30 ± 1 sr, slightly higher than those typical for marine conditions (20–25 sr) (Müller et al., 2007; Córdoba-Jabonero et al., 2011). This result can be related to marine mixtures with other particles with predominance of sea salt aerosols. On 31 July, a daily-averaged value of 38 ± 8 sr was obtained applying a 'pure dust scenario' retrieval to lidar measurements with AOD^{IZO} convergence (Córdoba-Jabonero et al., 2014), since dust was confined mostly in the FT layer. However, the situation on this day corresponded to a weak progressively arriving dust intrusion with low dust loading present along the day, as also reflected by both the AERONET AOD data found for this day (a mean value of 0.17 ± 0.07 was reported) and the backtrajectories coming from Sahara area only arriving at altitudes higher than 3000 m a.g.l. (see Fig. 2). In particular, LR values derived from Lidar profiles registered between 10:00 and 12:00 UTC, coincident with the time interval of aircraft measurements, were within the 31–50 sr range, being the last value closer to those LRs reported for Saharan dust occurrence (Müller et al., 2007; Córdoba-Jabonero et al., 2011, 2016; Schuster et al., 2012). This difference shows the variability of DD conditions along this day. As previously stated, a strong dust intrusion occurs on 01 August 2013 (AERONET AODs of 1.43 ± 0.06 are found, see Section 3.1), corresponding to a daily-averaged LR of 51 ± 16 sr. This result indicates that typical values for pure Saharan dust remained along the overall day unlike the previous day (31 July). Similarly, LR ranged for the simultaneous lidar measurements with aircraft flights between 53 and 55 sr, representative LR values for pure Saharan dust particles.

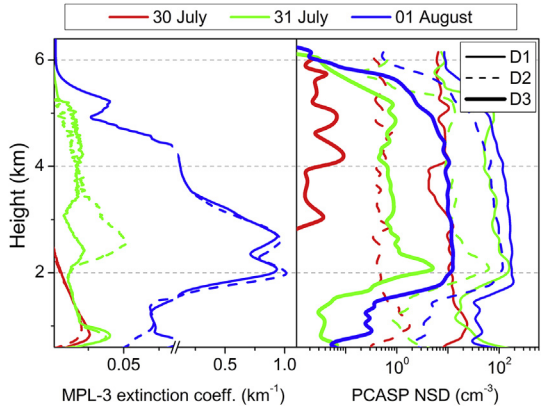

Fig. 3. Simultaneous height-resolved measurements. (Left) Lidar-derived extinction coefficients (hourly-averaged at 10:00–11:00 UTC (solid line) and 11:00–12:00 UTC (dashed line) on 30 July (red), 31 July (green) and 01 August (blue) 2013. (Right) PCASP particle number size distributions (NSD) at selected size ranges (D1, D2 and D3 are shown by solid thin, dashed and solid thick lines, respectively) for those days (colour lines correspond to the same days as shown in left panel). A NSD detection limit of 10^{-2} cm^{-3} is shown. (For interpretation of the references to colour in this figure legend, the reader is referred to the web version of this article.)

3.3. Total mass concentration of Saharan dust particles

The Total Mass Concentration (TMC) is obtained directly by applying Eq. (3), assuming a MEE value of 1.0 m^2 g^{-1}, as that reported for dust in Morocco (African zone closer to our sampling site, see Table 1). Mass Concentration MC for particles within both the fine (D1+D2) and coarse (D3 and D4) modes are also calculated

Table 2
Extinction and NSD increases at FT/BL layers with respect to the ND case for the examined 3-day period.

	30 July (ND)	31 July (DD)	01 August (DD)
	FT/BL	FT/BL	FT/BL
Airborne data: NSD			
D1 (fine mode)	1 / 1	7 / 1.9	11 / 1.5
D2 (fine mode)	1 / 1	24 / 1.2	101 / 1.4
D3 (coarse mode)	1 / 1	53 / 1.7	448 / 3.0
Lidar data			
Extinction	1 / 1	7 / 1.4	140 / 3.7
LR (sr)	Daily	Daily (flight time)	Daily (flight time)
	30 ± 1	38 ± 8 (31 ÷ 50)	51 ± 16 (53 ÷ 55)

as previously stated in Section 2.5. A vertical TMC estimate is shown in Fig. 4 together to the mass concentration of particles within the fine (D1 + D2) and coarse (D3 and D4) modes (Fig. 4, left panel). In particular, the D4 particle mode was calculated as the difference between the TMC and the MC for the extended fine-to-coarse (D1 + D2 + D3) mode, as exposed in Section 2.5. Fig. 4 also shows the MC for particles registered by PCASP in each D1, D2 and D3 size range (Fig. 4, right panel).

The MC within each PCASP size range (D1, D2 and D3) shows the dust layer confined mostly at FT altitudes, between 1.7 and 6 km height, likewise as exposed in Section 3.2. Despite the amount of particles with larger diameters is lower (see Fig. 3, right), their contribution to the MC is enhanced (see Fig. 4, right) during the DD event, as expected; in particular, the MC in each PCASP channel increases at FT altitudes from 31 July to 01 August with respect to ND conditions. Table 3 shows the MC values (in μg m^{-3}) at around 4 km height, for instance, for each PCASP D1, D2 and D3 size range on 30 July, 31 July and 01 August, respectively. A similar behaviour is observed for the total mass concentration TMC evaluated by using the dust extinction data (see Table 3 and Fig. 4, left). Therefore, dust incidence is mostly affecting the MC of larger particles.

Regarding the DD situation on 31 July, the contribution to TMC of large D4 particles is observed at both BL and FT altitudes, while particles with diameter smaller than 2.8 μm are mainly observed in the FT. However, special attention should be paid to the layer ranging from 1.8 to 2.4 km height, since the estimated mass concentration of all the particles is lower than that for particles with diameter lower than 2.8 μm (D1 + D2 + D3). Indeed, this inconsistency highlights the fact that TMC could be not correctly evaluated for this layer. Neglecting that the errors in the airborne and ground-based measurements could be causing this anomaly in the calculation of mass concentrations, the actual values for MEE rather than for particle density (see Eqs. (2) and (3)) in this particular atmospheric layer can be different from those assumed in this work (see Section 2.5). In particular, the actual TMC can be higher by using a MEE value lower than that assumed (i.e., 1.0 m^2 g^{-1}). In general, MEE for dust depends on the predominant particle mode. Tegen and Lacis (1996), modelling the particle size distributions to estimate their influence in the radiative properties of mineral dust, reported MEE values from 3.1 (fine particles) to 0.16 (coarse particles) m^2 g^{-1}. Hence, our results reflect the predominance of considerably larger particles (represented by lower MEEs) in this layer (1.8–2.4 km height). Unfortunately, the PCASP cut-off size detection limit is found for particles with diameters higher than 2.8 μm (unregistered D4 particles), and hence a suitable MEE value (lower than 1.0 m^2 g^{-1}, as assumed) is unable to be accurately estimated for this particular layer.

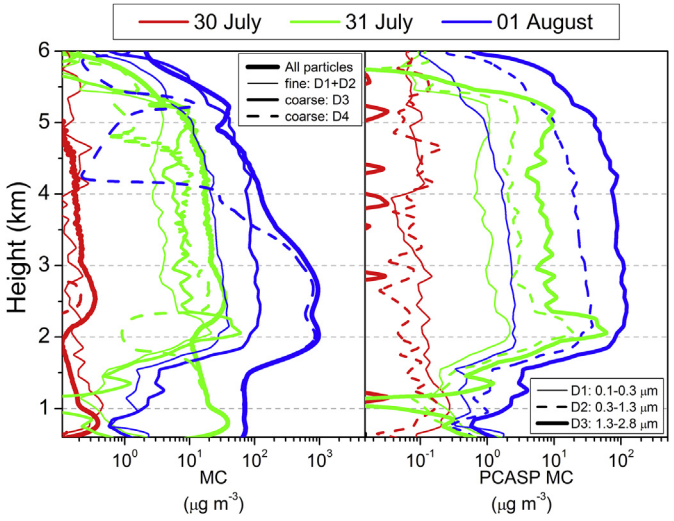

Fig. 4. (Left) Vertical TMC estimate (μg m^{-3}) at the time of airborne measurements (solid thick lines) on 30 July (red), 31 July (green) and 01 August (blue), together to the vertical MC (μg m^{-3}) for particles within both the fine (D1 + D2) (solid thin lines) and coarse (D3 and D4) modes (solid and dashed lines, respectively). (Right) Vertical MC (μg m^{-3}) for particles registered by PCASP, as detached in the D1 (solid thin lines), D2 (dashed lines) and D3 (solid thick lines) size ranges (a particle density of 2.0 g cm^{-3} is assumed). Colour lines correspond to the same days as shown in the left panel. (For interpretation of the references to colour in this figure legend, the reader is referred to the web version of this article.)

In the case of the strong dust intrusion on 01 August, the TMC up to 3.6 km height is likely linked only to the contribution of the no-collected coarse mode particles (D4 particles); at higher altitudes, the mass contribution of the smaller particles (fine and D3 mode) to the TMC is particularly enhanced. These results indicate a predominance of particles larger than 2.8 μm size at lower FT altitudes than 3.6 km height, likewise smaller than 2.8 μm particles are found at higher altitudes, contributing both to the total mass concentration TMC during the strong dust case. Hence, a selective contribution by the particle size is clearly observed on 01 August, likely due to gravitational settling processes of large particles.

The impact on mass concentration within the BL was weaker than in the FT, as also observed in previous results (see Fig. 3). In particular, the MC in the BL increases with respect to ND conditions, but this increase rate is lower than that observed at FT altitudes. For instance, TMC and the MC (in μg m^{-3}) for each D1, D2 and D3 size range at around 1.2 km height on 30 July, 31 July and 01 August is shown in Table 3. In general, as mass concentration increases as particle size is higher. Indeed, the primary contribution to the MC in the BL is due to rather larger particles on both 31 July and 01 August 2013 (see Fig. 4, left). The comparison of the MC obtained by using the PCAPS (D1+D2) fine mode particles (see Fig. 4, left) over Tenerife area with those obtained during the PRIDE experiment (Reid et al., 2003) shows similar mass concentration levels under background ND conditions and during the weak dust intrusion on 31 July. In the case of the strong dust intrusion on 01 August, the dust impact over Tenerife was rather higher. Indeed, unlike the PRIDE campaign, these high dust loading levels were particularly present during the AMISOC-TNF strong dust intrusion case.

Near-surface MC are also shown in Table 3 in order to indicate the potential air quality impact in total suspended particles (TSP) levels. Hence, TMC of around 9 and 21 μg m^{-3} are found at 400 m height, respectively, on 31 July and 01 August 2013.

3.4. Evaluation of MAXDOAS extinction profiling retrieval

Parameters characterizing the aerosol profile retrieval from MAXDOAS measurements have been chosen carefully after several tests. In this work, $\boldsymbol{y}$ represents the measured MAXDOAS O_4 DSCD, and $\mathbf{S}_\varepsilon$ is set to a diagonal matrix with their diagonal elements corresponding to the molecular errors of the measurements (see Eq. (1)). In addition, atmospheric parameters were obtained from the

Table 3
Mass concentration MC (μg m^{-3}) at specific altitudes within the BL and FT (1.2 and 4.0 km height, respectively) and on the near-surface level for each PCASP channel and the TMC as obtained from extinction Lidar data.

	30 July (ND)	31 July (DD)	01 August (DD)
	FT (4.0 km) / BL (1.2 km) / near-surface (0.4 km)		
D1 (fine mode)	0.06 / 0.23 / 2.0	0.7 / 0.16 / 3.4	1.7 / 0.4 / 2.8
D2 (fine mode)	0.07 / 0.11 / 1.2	2.0 / 0.14 / 1.1	19.5 / 0.9 / 0.9
D3 (coarse mode)	0.015 / 0.02 / 0.2	5.6 / 0.27 / 2.4	75.0 / 3.2 / 0.8
TMC	1.6 / 1.8 / 3.6	15.5 / 18.3 / 8.6	124 / 70 / 21

standard atmosphere for tropical latitudes (Anderson, 1986), being the atmospheric column stratified into layers of 200 m from the IZO station level (2370 m a.s.l. height) up to 3.9 km, layers of 600-m thickness from 3.9 to 6.3 km height and over 8 km layers of the same width as those corresponding to the standard atmosphere for tropical latitudes. The retrieved profiles were calculated at 477 nm, and at altitudes up to 6.3 km height, since the OEM sensitivity to the measurements is reduced over this altitude. **K** matrix was calculated with the LIDORT (Linearized Discrete Ordinate Radiative Transfer) radiative transfer model (Spurr, 2008). The a priori aerosol extinction profile applied was an exponential function decreasing with altitude adjusted to an extinction value of 0.02 km^{-1} at the IZO height level and nearby zero close to 6 km height. Diagonal $\mathbf{S_a}$ elements are usually chosen to be a percentage of $\boldsymbol{x_a}$, being set to 40% of $\boldsymbol{x_a}$, and its non-diagonal elements were calculated following the expression (Barret et al., 2002; Friess et al., 2006):

$$S_{aij} = \sqrt{S_{aii}S_{ajj}}\exp(-\ln 2)\left(\left(\left(z_i - z_j\right)/\gamma\right)^2\right) \quad (4)$$

where z_i and z_j are the heights of the altitude grid levels, i and j respectively, and γ is a half of the correlation length. In this work, a value of 500 m was fixed for γ. Functions S_{aij} in Eq. (4) are Gaussian correlation functions that account for correlations between trace gas concentrations at different altitudes.

Aerosol extinction provided by the OEM approach at a given altitude is actually an average of the total extinction profile weighted by the corresponding row of the so-called Averaging Kernel matrix **A**. This matrix expresses the sensitivity of the retrieval to the true state, playing a determinant role in the characterization of the retrieval. **A** is described by the following expression:

$$A = G_y K, \quad (5)$$

where the gain matrix $\mathbf{G_y}$ quantifies the sensitivity of the retrieval to the measurements, i.e.,

$$G_y = S_a K^T \left(K S_a K^T + S_\in\right)^{-1}. \quad (6)$$

In general, the **A** rows are functions with a single peak at the appropriate height-level, where the measurement provides additional information to add to the a priori selected profile.

Lidar extinction profiles (ε_L) are characterized by a much higher vertical resolution than MAXDOAS profiling retrievals. Hence, the extinction profiles obtained by both RS techniques could be only qualitatively compared. In order to properly compare both (MAXDOAS and Lidar) aerosol extinction profiles, the Lidar values coincident in altitude with those obtained by the OEM retrieval were only used, being additionally smoothed (ε_L') by using the **A** functions, i.e.,

$$\varepsilon_L' = A\varepsilon_L. \quad (7)$$

Fig. 5 shows lidar extinction profiles on days 31 July (left panel) and 1 August (right panel) 2013 as obtained before (black lines) and after (red lines) applying that smoothing procedure, in comparison with those obtained from O_4-based MAXDOAS measurements (green lines). Results indicate that both MAXDOAS and Lidar extinction profiles present a relatively good agreement, once that specific smoothing is applied to Lidar measurements. Indeed, general features observed in the smoothed Lidar extinction profiles are well reproduced by those derived from MAXDOAS retrievals, taking into account the limitations of both techniques.

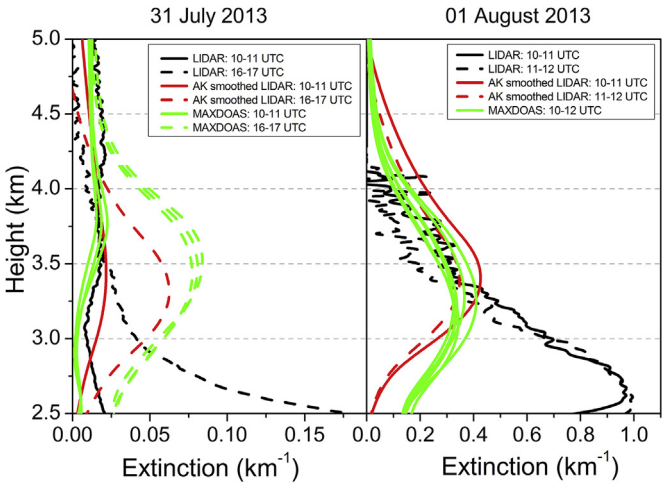

Fig. 5. Extinction profiles between 10:00–11:00 (case A) and 16:00–17:00 UTC (case B) on 31 July (left), and between 10:00–12:00 UTC (case C) on 1 August 2013 (right) derived by: MAXDOAS retrieval (green lines), and LIDAR inversion before (black lines) and after (red lines) Averaging Kernel smoothing. (For interpretation of the references to colour in this figure legend, the reader is referred to the web version of this article.)

In particular, three cases are examined (see Fig. 5). On 31 July between 10:00 and 11:00 UTC (case A), all the extinction profiles show low values, as expected since the dust intrusion only partially reached the IZO station. Later on the same day between 16:00 and 17:00 UTC (case B), when Saharan dust intrusion arrives completely to IZO site, a dust layer with higher extinction values extending from the station (around 2.4 km a.s.l.) up to 4.2 km height is observed by both instruments. Maximal smoothed lidar extinction values (about 0.06 km^{-1}) are found at around 3.4 km a.s.l., whereas close to these values (about 0.08 km^{-1}) are derived by MAXDOAS at around 3.6 km height. Next day, on 01 August between 10:00 and 12:00 UTC (case C), the stronger Saharan dust intrusion is observed also by both RS techniques, showing a good agreement between the maximal extinction values found, ranging from 0.33 to 0.44 km^{-1} at around 3.2–3.4 km height, for both profiling datasets.

In addition, root-mean-squared differences (RMSD) were calculated for smoothed lidar and MAXDOAS averaged profiles, obtaining values of 0.008, 0.019 and 0.086 for cases A, B and C, respectively. This apparent RMSD growth seems to be related to the dust loading (or AOD) increase observed over IZO site during this 2-day DD period, since AOD values at IZO of 0.06, 0.18 and 0.95 were also reported for cases A, B and C, respectively; in particular, the lower extinction values were found for case A (low AOD), presenting also the lower RMSD. These results can reflect indeed the aerosol loading effect in both the MAXDOAS technique and retrieval. Furthermore, observed differences can be also associated to the fact that MAXDOAS measurements are averaged over large horizontal distances (i.e., up to tens of kilometres), whereas the lidar instrumentation provides measurements directly over the sampling site.

Therefore, although these first results are rather valuable for MAXDOAS-derived dust extinction profiling assessment, a much longer period of MAXDOAS measurements under Saharan dust occurrence must be analyzed to actually confirm this AOD-RMSD relationship for MAXDOAS retrievals. Hence, a more detailed work is on-going.

4. Conclusions

Dusty (DD) conditions occurring during AMISOC-TNF campaign have been analyzed in terms of the microphysical and optical properties of Saharan dust particles. In particular, the DD situation

corresponding to a progressively arriving Saharan dust intrusion over Tenerife area on 31 July 2013 (weak incidence), remaining along the following day (01 August) with strong incidence, has been especially examined in this work by using simultaneous airborne in-situ and remote sensing lidar measurements. This dust intrusion was identified by both AERONET data (AOD and AEx values, respectively, ranged from 0.2 to 0.35 to 1.5 and 0.05, for these two days) and HYSPLIT backtrajectory analysis confirming also its Saharan origin. As a reference, the background non-dusty (ND) case occurred on the previous day (30 July) corresponded to clean air masses coming from the Atlantic Ocean with AOD and AEx values of 0.03 and 1.1, respectively.

Vertical profiles of both dust extinction and mass concentration were derived, respectively, from lidar measurements and airborne particle size distributions (SD) for three particle size ranges within the fine and partial coarse modes. Both the optical and microphysical profilings show dust particles confined in a wide layer of 4.3 km thickness ranging from 1.7 to 6 km height. LR ranged between 50 and 55 sr, showing typical values for Saharan dust. Dust incidence mostly affected FT altitudes, being rather lower in the BL, as reflected by both the lidar and airborne measurements.

In general, during this 2-day DD period, the dust impact on mass concentration was enhanced due to the increasing dust loading of larger particles, affecting both the BL and FT, but showing differences depending on the dusty case. On 31 July (weak dust intrusion), the contribution of both fine and coarse particles is observed at FT altitudes higher than 2.4 km, but only large particles seem to be present at lower heights, covering the BL. Though, these large BL aerosols can be mixtures of dust particles with likely marine aerosols, since the arrival of Saharan air masses is observed only at altitudes higher than 3000 m a.g.l. on this day, as corroborated by HYSPLIT backtrajectory analysis. Hence, the presence of dust particles in the BL is likely due to gravitational processes from higher altitudes. In addition, the use of an averaged MEE value to be assumed for vertical total mass concentration estimation is especially critical for particular layers, and those cases must be examined in detail. On 01 August (strong dust intrusion), however, air masses were coming from the Sahara region mostly at altitudes higher than 1000 m a.g.l. This indicates clearly a selective contribution with altitude depending on the particle size, likely due to gravitational settling of larger particles into the BL. In particular, a higher incidence of larger dust particles is observed in the FT from 1.7 km height up to 3.6 km height; from this altitude up, the contribution of smaller dust particles is enhanced. Indeed, the synergy between lidar retrievals and airborne in-situ measurements is demonstrated for estimating the height-resolved mass concentration of Saharan dust particles. In addition, the results of our study point out the importance of dust impact within the BL and FT and the different contributions of fine and coarse dust particles, affecting the total suspended particulate (TSP) levels on surface. Indeed, this is particularly relevant for both air quality assessment and health effect concerns of dust particles.

Moreover, the potential of the MAXDOAS technique to provide aerosol profiling retrievals has been especially highlighted in this preliminary work, showing a good agreement with the lidar-derived extinction profiles, once the Averaging Kernel smoothing procedure is applied. Hence, a MAXDOAS-lidar validation study using a more extended period of DD cases is on-going.

Acknowledgements

This work is supported by the Spanish Ministerio de Economía y Competitividad (MINECO) under grants CGL2011-24891 and CGL2014-55230-R. Authors specially thank to O. Serrano and N. Seoane (INTA) for airborne instrumentation support. Authors are grateful to the INTA Aerial platforms (Spanish ICTS program) and the Spanish Air Force (CLAEX unit) for theirs efforts in maintaining and operating the aircrafts. We acknowledge the NOAA Air Resources Laboratory for the provision of the HYSPLIT model. Authors thank AEMET (Spanish State Meteorological Agency) and European Centre for Medium-Range Weather Forecasts (ECMWF) for the access to the input meteorological fields.

References

Amiridis, V., Wandinger, U., Marinou, E., Giannakaki, E., Tsekeri, A., Basart, S., Kazadzis, S., Gkikas, A., Taylor, M., Baldasano, J., Ansmann, A., 2013. Optimizing CALIPSO Saharan dust retrievals. Atmos. Chem. Phys. 13, 12089–12106.

Anderson, G.P., 1986. AFGL Atmospheric Constituent Profiles (0-120 Km), Hanscom AFB, MA: AFGL-TR; 86-0110. U.S. Air Force Geophysics Laboratory. Optical Physics Division.

Ansmann, A., Petzold, A., Kandler, K., Tegen, I., Wendisch, M., Müller, D., Weinzierl, B., Müller, T., Heintzenberg, J., 2011. Saharan mineral dust experiments SAMUM-1 and SAMUM-2: what have we learned? Tellus 63B, 403–429.

Barret, B., De Maziere, M.D., Demoulin, P., 2002. Retrieval and characterization of ozone profiles from solar infrared spectra at the Jungfraujoch. J. Geophys. Res. 107 (D24), 4788. http://dx.doi.org/10.1029/2001JD001298.

Baumgardner, D., Jonsson, H., Dawson, W., O'Connor, D., Newton, R., 2001. The Cloud, Aerosol and precipitation spectrometer: a new instrument for cloud investigations. Atmos. Res. 59–60, 251–264.

Baumgardner, D., Raga, G.B., Jimenez, J.C., Bower, K., 2005. Aerosol particles in the mexican east pacific Part I: processing and vertical redistribution by clouds. Atmos. Chem. Phys. 5, 3081–3091. http://dx.doi.org/10.5194/acp-5-3081-2005.

Boucher, O., Randall, D., Artaxo, P., Bretherton, C., Feingold, G., Forster, P., Kerminen, V.-M., Kondo, Y., Liao, H., Lohmann, U., Rasch, P., Satheesh, S.K., Sherwood, S., Stevens, B., Zhang, X.Y., 2013. Clouds and aerosols. In: Stocker, T.F., Qin, D., Plattner, G.-K., Tignor, M., Allen, S.K., Boschung, J., Nauels, A., Xia, Y., Bex, V., Midgley, P.M. (Eds.), Climate Change 2013: the Physical Science Basis. Contribution of Working Group I to the Fifth Assessment Report of the Intergovernmental Panel on Climate Change. Cambridge University Press, Cambridge, United Kingdom and New York, NY, USA.

Cai, Y., Snider, J.R., Wechsler, P., 2013. Calibration of the passive cavity aerosol spectrometer Probe for airborne determination of the size distribution. Atmos. Meas. Tech. 6 (9), 2349–2358.

Campbell, J.R., Hlavka, D.L., Welton, E.J., Flynn, C.J., Turner, D.D., Spinhirne, J.D., Stanley Scott III, V., Hwang, I.H., 2002. Full-time, eye-safe cloud and aerosol Lidar observation at atmospheric radiation measurement program sites: instruments and data processing. J. Atmos. Ocean. Technol. 19, 431–442.

Campbell, J.R., Tackett, J.L., Reid, J.S., Zhang, J., Curtis, C.A., Hyer, E.J., Sessions, W.R., Westphal, D.L., Prospero, J.M., Welton, E.J., Omar, A.H., Vaughan, M.A., Winker, D.M., 2012. Evaluating nighttime CALIOP 0.532 μm aerosol optical depth and extinction coefficient retrievals. Atmos. Meas. Tech. 5, 2143–2160.

Carlson, T.N., Prospero, J.M., 1972. The large-scale movement of Saharan air outbreaks over the northern Equatorial Atlantic. J. Appl. Meteor. 11, 283–297.

Chen, G., Ziemba, L.D., Chu, D.A., Thornhill, K.L., Schuster, G.L., Winstead, E.L., Diskin, G.S., Ferrare, R.A., Burton, S.P., Ismail, S., Kooi, S.A., Omar, A.H., Slusher, D.L., Kleb, M.M., Reid, J.S., Twohy, C.H., Zhang, H., Anderson, B.E., 2011. Observations of Saharan dust microphysical and optical properties from the eastern Atlantic during NAMMA airborne field campaign. Atmos. Chem. Phys. 11, 723–740. http://dx.doi.org/10.5194/acp-11-723-2011.

Clémer, K., Van Roozendael, M., Fayt, C., Hendrick, F., Hermans, C., Pinardi, G., Spurr, R., Wang, P., De Mazière, M., 2010. Multiple wavelength retrieval of tropospheric aerosol optical properties from MAXDOAS Measurements in Beijing. Atmos. Meas. Tech. 3, 863–878. http://dx.doi.org/10.5194/amt-3-863-2010.

Córdoba-Jabonero, C., Sorribas, M., L.Guerrero-Rascado, J., Adame, J.A., Hernández, Y., Lyamani, H., Cachorro, V., Gil, M., Alados-Arboledas, L., Cuevas, E., de la Morena, B., 2011. Synergetic monitoring of Saharan dust plumes and potential impact on surface: a case study of dust transport from Canary Islands to Iberian Peninsula. Atmos. Chem. Phys. 11, 3067–3091. http://dx.doi.org/10.5194/acp-11-3067-2011.

Córdoba-Jabonero, C., Adame, J.A., Grau, D., Cuevas, E., Gil, M., 2014. Lidar Ratio discrimination retrieval in a two-layer aerosol system from elastic lidar measurements in synergy with sun-photometry data. In: Proceedings of the International Conference in Atmospheric Dust (DUST 2014), ProScience, vol. 1. Published by Digilabs, pp. 243–248. http://dx.doi.org/10.14644/dust.2014.040.

Córdoba-Jabonero, C., Adame, J.A., Campbell, J.R., Cuevas, E., Díaz, J.P., Expósito, F, Gil-Ojeda, M., 2016. Lidar Ratio derived for pure dust aerosols: Multi-year Micro Pulse Lidar observations in a Saharan dust-Influenced region. EPJ Web Conf. 119, 23017. http://dx.doi.org/10.1051/epjconf/201611923017.

de la Paz, D., Vedrenne, M., Borge, R., Lumbreras, J., de Andrés, J.M., Pérez, J., Rodríguez, E., Karanasiou, A., Moreno, T., Boldo, E., Linares, C., 2013. Modelling Saharan dust transport into the Mediterranean basin with CMAQ. Atmos. Environ. 70, 337–350.

Draxler, R.R., Stunder, B., Rolph, G., Taylor, A., 2009. HYSPLIT_4 User's Guide, via NOAA ARL Website. NOAA Air Resources Laboratory, Silver Spring, MD. December 1997, revised January 2009. http://www.arl.noaa.gov/documents/

reports/hysplit_user_guide.pdf.
d'Almeida, G.A., Koepke, P., Shettle, E.P., 1991. Atmospheric Aerosols: Global Climatology and Radiative Characteristics. A. Deepak Publishing, Hampton, VA.
Fernald, F.G., 1984. Analysis of atmospheric lidar observations: some comments. Appl. Opt. 23, 652–653.
Formenti, P., Rajot, J.L., Desboeufs, K., Saïd, F., Grand, N., Chevaillier, S., Schmechtig, C., 2011. Airborne observations of mineral dust over western Africa in the summer Monsoon season: spatial and vertical variability of physico-chemical and optical properties. Atmos. Chem. Phys. 11, 6387–6410.
Friess, U., Monks, P., Remedios, J., Rozanov, A., Sinreich, R., Wagner, T., Platt, U., 2006. MAX-DOAS O_4 measurements: a new technique to derive information on atmospheric aerosols: 2. Modeling studies. J. Geophys. Res. 111. D14203.
Gil, M., Yela, M., Gunn, L.N., Richter, A., Alonso, I., Chipperfield, M.P., Cuevas, E., Iglesias, J., Navarro, M., Puentedura, O., Rodríguez, S., 2008. NO_2 climatology in the northern subtropical region: diurnal, seasonal and interannual variability. Atmos. Chem. Phys. 8, 1635–1648. http://dx.doi.org/10.5194/acp-8-1635-2008.
Hendrick, F., Müller, J.-F., Clémer, K., Wang, P., De Mazière, M., Fayt, C., Gielen, C., Hermans, C., Ma, J.Z., Pinardi, G., Stavrakou, T., Vlemmix, T., Van Roozendael, M., 2014. Four years of ground-based MAX-DOAS observations of HONO, and NO2 in the Beijing area. Atmos. Chem. Phys. 14, 765–781.
Hess, M., Koepke, P., Schult, I., 1998. Optical properties of aerosols and clouds: the software package OPAC. Bull. Am. Meteorol. Soc. 79, 831–844.
Holben, B.N., Tanré, D., Smirnov, A., Eck, T.F., Slutsker, I., Abuhassan, N., Newcomb, W.W., Schafer, J.S., Chatenet, B., Lavenu, F., Kaufman, Y.J., Vande Castle, J., Setzer, A., Markham, B., Clark, D., Frouin, R., Halthore, R., Karneli, A., O'Neill, N.T., Pietras, C., Pinker, R.T., Voss, K., Zibordi, G., 2001. An emerging ground-based aerosol climatology: aerosol optical depth from AERONET. J. Geophys. Res. 106 (D11), 12067–12097.
Kandler, K., Schütz, L., Deutscher, C., Ebert, M., Hofmann, H., Jäckel, S., Jaenicke, R., Knippertz, P., Lieke, K., Massling, A., Petzold, A., Schladitz, A., Weinzierl, B., Wiedensohler, A., Zorn, S., Weinbruch, S., 2009. Size distribution, mass concentration, chemical and mineralogical composition and derived optical parameters of the boundary layer aerosol at Tinfou, Morocco, during SAMUM 2006. Tellus 61B, 32–50.
Klett, J.D., 1985. Lidar inversion with variable backscatter/extinction ratios. Appl. Opt. 24, 1638–1643.
Li, X., Maring, H., Savoie, D., Voss, K., Prospero, J.M., 1996. Dominance of mineral dust in aerosol light-scattering in the North Atlantic trade winds. Nature 380, 416–419.
Maring, H., Savoie, D.L., Izaguirre, M.A., McCormick, C., Arimoto, R., Prospero, J.M., Pilinis, C., 2000. Aerosol physical and optical properties and their relationship to aerosol composition in the free troposphere at Izaña, Tenerife, Canary Islands, during July 1995. J. Geophys. Res. 105 (D11), 14677–14700. http://dx.doi.org/10.1029/2000JD900106.
Molero, F., Andrey, F.J., Fernandez, A.J., Parrondo, M.C., Pujadas, M., Córdoba-Jabonero, C., Revuelta, M.A., Gomez-Moreno, F.J., 2014. Study of vertically resolved aerosol properties over an urban background site in Madrid (Spain). Int. J. Remote Sens. 35 (6), 2311–2326.
Müller, D., Ansmann, A., Mattis, I., Tesche, M., Wandinger, U., Althausen, D., Pisani, G., 2007. Aerosol-type-dependent lidar ratios observed with Raman lidar. J. Geophys. Res. 112 http://dx.doi.org/10.1029/2006JD008292. D16202.
Myhre, G., Shindell, D., Bréon, F.-M., Collins, W., Fuglestvedt, J., Huang, J., Koch, D., Lamarque, J.-F., Lee, D., Mendoza, B., Nakajima, T., Robock, A., Stephens, G., Takemura, T., Zhang, H., 2013. Anthropogenic and natural radiative forcing. In: Stocker, T.F., Qin, D., Plattner, G.-K., Tignor, M., Allen, S.K., Boschung, J., Nauels, A., Xia, Y., Bex, V., Midgley, P.M. (Eds.), Climate Change 2013: the Physical Science Basis. Contribution of Working Group I to the Fifth Assessment Report of the Intergovernmental Panel on Climate Change. Cambridge University Press, Cambridge, United Kingdom and New York, NY, USA.
Platt, U., Stutz, J., 2008. Differential Optical Absorption Spectroscopy: Principles and Applications. Springer-Verlag, Berlin, Germany.
Puentedura, O., Gil, M., Saiz-Lopez, A., Hay, T., Navarro-Comas, M., Gómez-Pelaez, A., Cuevas, E., Iglesias, J., Gomez, L., 2012. Iodine monoxide in the north subtropical free troposphere. Atmos. Chem. Phys. 12, 4909–4921. http://dx.doi.org/10.5194/acp-12-4909-2012.
Reid, J.S., Kinney, J.E., Westphal, D.L., Holben, B.N., Welton, E.J., Tsay, S.Ch., Eleuterio, D.P., Campbell, J.R., Christopher, S.A., Colarco, P.R., Jonsson, H.H., Livingston, J.M., Maring, H.B., Meier, M.L., Pilewskie, P., Prospero, J.M., Reid, E.A., Remer, L.A., Russell, P.B., Savoie, D.L., Smirnov, A., Tanre, D., 2003. Analysis of measurements of Saharan dust by airborne and ground-based remote sensing methods during the Puerto Rico Dust Experiment (PRIDE). J. Geophys. Res. 108 (D19), 8586. http://dx.doi.org/10.1029/2002JD002493.
Rodgers, C.-D., 1990. Characterization and error analysis of profiles retrieved from remote sounding measurements. J. Geophys. Res. 95, 5587–5595.
Rosenberg, P.D., Dean, A.R., Williams, P.I., Dorsey, J.R., Minikin, A., Pickering, M.A., Petzold, A., 2012. Particle sizing calibration with refractive index correction for light scattering optical particle counters and impacts upon PCASP and CDP data collected during the Fennec campaign. Atmos. Meas. Tech. 5, 1147–1163.
Schepanski, K., Tegen, I., Macke, A., 2009. Saharan dust transport and deposition towards the tropical northern Atlantic. Atmos. Chem. Phys. 9, 1173–1189. http://dx.doi.org/10.5194/acp-9-1173-2009.
Schuster, G.L., Vaughan, M., MacDonnell, D., Su, W., Winker, D., Dubovik, O., Lapyonok, T., Trepte, C., 2012. Comparison of CALIPSO aerosol optical depth retrievals to AERONET measurements, and a climatology for the lidar ratio of dust. Atmos. Chem. Phys. 12, 7431–7452. http://dx.doi.org/10.5194/acp-12-7431-2012.
Spurr, R., 2008. LIDORT and VLIDORT: linearized pseudo-spherical scalar and vector discrete ordinate radiative transfer models for use in remote sensing retrieval problems. In: Kokhanovsky, A. (Ed.), Light Scattering Reviews 3, Springer Praxis Books, vol. 7. Springer, Berlin Heidelberg, pp. 229–275. http://dx.doi.org/10.1007/978-3-540-48546-9.
Tegen, I., Lacis, A., 1996. A.: modeling of particle size distribution and its influence on the radiative properties of mineral dust aerosol. J. Geophys. Res. 101, 19237–19244. http://dx.doi.org/10.1029/95JD03610.
Toledano, C., Cachorro, V.E., Berjón, A., de Frutos, A.M., Sorribas, M., de la Morena, B.A., Goloub, P., 2007a. Aerosol optical depth and Ångström exponent climatology at El Arenosillo AERONET site (Huelva, Spain). Q.J.R. Meteorol. Soc. 133, 795–807. http://dx.doi.org/10.1002/qj.54.
Toledano, C., Cachorro, V.E., De Frutos, A.M., Sorribas, M., Prats, N., De la Morena, B.A., 2007b. Inventory of African desert dust events over the south-western iberian peninsula in 2000-2005 with an AERONET cimel sun photometer. J. Geophys. Res. 112 http://dx.doi.org/10.1029/2006JD008307. D21201.
Wagner, T., Dix, B., Friedeburg, V.C., Friess, U., Sanghavi, S., Sinreich, R., Platt, U., 2004. MAX-DOAS O4 measurements: a new technique to derive information on atmospheric aerosols principles and information content. J. Geophys. Res. 109 http://dx.doi.org/10.1029/2004JD004904. D22205.
Weinzierl, B., Petzold, A., Esselborn, M., Wirth, M., Rasp, K., Kandler, K., Schütz, L., Koepke, P., Fiebig, M., 2009. Airborne measurements of dust layer properties, particle size distribution and mixing state of Saharan dust during SAMUM 2006. Tellus B 61, 96–117.
Zhang, L., Li, Q.B., Gu, Y., Liou, K.N., Meland, B., 2013. Dust vertical profile impact on global radiative forcing estimation using a coupled chemical-transport–radiative-transfer model. Atmos. Chem. Phys. 13, 7097–7114.